

# Detection of Incumbent Radar in the 3.5 GHz CBRS Band Using Support Vector Machines

Raied Caromi and Michael Souryal  
Communications Technology Laboratory  
National Institute of Standards and Technology  
Gaithersburg, Maryland, U.S.  
raied.caromi@nist.gov, souryal@nist.gov

**Abstract**—In the 3.5 GHz Citizens Broadband Radio Service (CBRS), 100 MHz of spectrum will be dynamically shared between commercial users and federal incumbents. Dynamic use of the band relies on a network of sensors dedicated to detecting the presence of federal incumbent signals and triggering protection mechanisms when necessary. This paper uses field-measured waveforms of incumbent signals in and adjacent to the band to evaluate the performance of support vector machine (SVM) classifiers for these sensors. We find that a peak analysis classifier and a higher-order statistics classifier perform comparably when the signal is in white Gaussian noise or commercial long term evolution (LTE) emissions, but with out-of-band emissions of adjacent-band systems the peak analysis classifier is far superior. This result also highlights the importance of including adjacent-band emissions in any performance evaluation of 3.5 GHz sensors.

**Index Terms**—3.5 GHz, CBRS, radar detection, machine learning, sensor

## I. INTRODUCTION

The Citizens Broadband Radio Service (CBRS) in the U.S. permits commercial broadband access to the radio frequency spectrum between 3550 MHz and 3700 MHz on a shared basis with incumbents in the band [1]. Among the incumbents is the U.S. military which operates radar systems in this band, including shipborne radar off the U.S. coasts. The CBRS rules permit dynamic access to the band in the proximity of military radar provided a sensor network detects the presence of the incumbent radar and triggers interference mitigation measures when necessary. The scope of this study is on the achievable detection performance of this sensor network.

In order to operate in the CBRS ecosystem, sensors must be able to detect the in-band incumbent radar signal at a minimum received power density of  $-89$  dBm (dB relative to 1 mW)/MHz [2], within 60 seconds of onset, and with a probability of detection of 99% or better [3]<sup>1</sup>. With this minimum required power density, the detection is clearly not thermal-noise-limited, as the detection threshold is 25 dB above the thermal noise floor. The challenge for detection is presented, rather, by co-channel interference.

There are two primary sources of co-channel interference at the sensor's receiver. First, by design, the band is shared with

commercial systems. Therefore, sensors must be able to detect the incumbent signal in channels occupied by commercial systems. These systems are expected to be LTE systems, at least initially. However, the emissions of commercial systems operating in the band can, in principle, be controlled by treating the sensors as protected entities in the CBRS ecosystem.

The second, more challenging, source of interference is the out-of-band emissions of systems operating in adjacent bands. These systems are also military radars, operate at frequencies below the CBRS band, and have been observed to generate significant emissions into the CBRS band [4], [5]. Detection by CBRS sensors differs from traditional radar detection primarily because the sensor aims to identify the presence of a radar signal rather than detecting and tracking a target. Additionally, unlike a typical radar receiver that has full access to the radar waveform, the sensor has only partial knowledge of radar waveform parameters. However, elements of classical radar detection can still be utilized. In prior related work, we evaluated coherent and non-coherent matched-filter detectors for this band [6]. Machine learning techniques have been used for cognitive radio and proposed for physical layer applications [7], [8]. Higher-order statistics and cumulant features were utilized for detection and classification in [9]–[11]. In addition, SVM and deep learning techniques were used for signal classification in [12]–[15].

This paper is a study of the performance of SVM classifiers trained to detect the current radar signal in the 3.5 GHz band. The analysis uses sets of training and evaluation waveforms derived from field measurements. Classifiers are trained on higher-order statistics of the signal amplitude as well as on temporal features of the peaks of the signal amplitude. The waveforms used for training and evaluation of the classifiers include field recordings of both the in-band radar and the out-of-band emissions of adjacent-band radars collected at two U.S. coastal locations [4], [5]. The field recordings were supplemented with computer-generated LTE signals and Gaussian noise. We present the achievable tradeoff between detection and false-alarm rates under different interference conditions for two SVM classifiers. While this study is limited to detection of the current in-band radar, SPN-43, a similar analysis can be performed for future radars deployed in this band.

<sup>1</sup>Government requirements do not specify a maximum probability of false alarm, although this figure of merit is naturally of interest to commercial users.

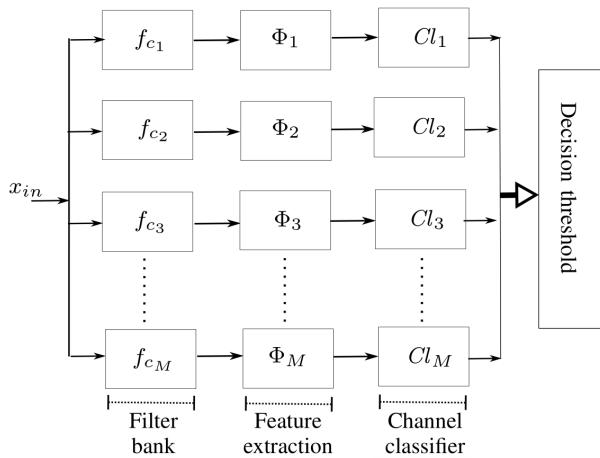


Fig. 1: Classification system overview

## II. SYSTEM MODEL

A sensor is responsible for detecting incumbent radar signals and identifying which 10 MHz channel each signal occupies within the lower 100 MHz of the band. One alternative is for a capable sensor to sample the entire 100 MHz and employ  $M$  filters to cover the entire bandwidth, each filter being centered at an appropriate frequency,  $f_{c_i}$ . The output of each filter is fed to a radar signal detector. The simplest form of a detector is a binary classifier indicating presence or absence of an incumbent radar signal. Fig. 1 demonstrates this configuration. In addition to filtering, the signal can be downsampled to an appropriate sampling rate,  $F_s$ , to reduce computations. After filtering, a set of features,  $\Phi_i$ , is extracted from the signal for use by a trained classifier  $Cl_i$  to decide whether the radar signal is present or absent in the channel.

For simplicity, we will assume that the classification branches are identical and thus we will drop the branch subscript  $i$  for the remainder. As in [6], the simplified signal model is given by

$$x[n] = s[n] + v[n],$$

where  $s$  is the in-band radar signal whose presence we are trying to detect, and  $v$  is either complex white Gaussian noise (CWGN), an LTE signal sharing the band, or adjacent-band interference (ABI) from radar emissions outside the band. The SVM classifier requires training before its use for detection. The model is trained on signal data that include scenarios similar to what a sensor will observe in field operation. The statistical hypothesis testing for the radar signal detection is

$$\begin{cases} H_0 : x[n] = v[n], \\ H_1 : x[n] = s[n] + v[n]. \end{cases}$$

Two probabilities are of interest for evaluating detection performance, the probability of false alarm,  $P_{FA} = Pr(\hat{H}_1|H_0)$ , and the probability of detection,  $P_D = Pr(\hat{H}_1|H_1)$ .

## III. SVM BINARY SIGNAL CLASSIFICATION

We model the detection problem of the incumbent radar signals as a binary classification problem. In supervised learning, the classifier requires the ground truth for the presence of the radar signal. Therefore, we generate training signal data with an appropriate response variable for the state of the incumbent radar signal. For both training and testing, all signals pass through a two-step normalization process. First, we subtract the mean of the signal from itself. This step reduces the direct current (DC) components in the signal. Second, we normalize the signal by its root mean square (RMS). RMS normalization removes the dependency of the extracted features on the magnitude of the signal.

### A. Feature extraction

For signal classification, the features are signal attributes that emphasize some phenomena of interest in the signal. Particularly, we are interested in signal features that are useful for detecting pulsed radar signals. Two examples of such signals with different types of background interference are shown in Fig. 2. In one case (Fig. 2a), the interference is an LTE signal and the pulsed radar signal is relatively easy to distinguish. In the other case (Fig. 2b), the interference also appears pulsed and detection is more challenging. We consider

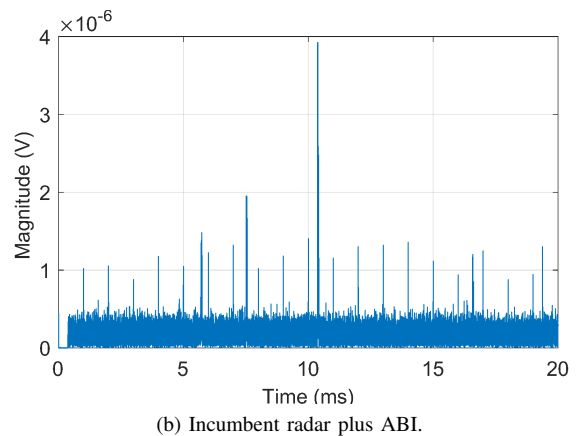
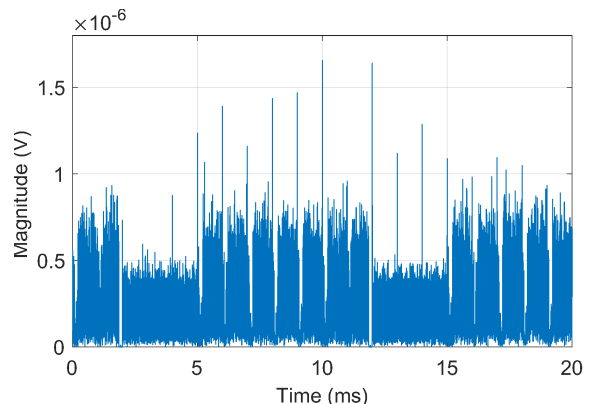


Fig. 2: Time domain radar signals plus interference.

two classification models, each with a distinct set of features extracted from the time-domain signals. One set is comprised of higher-order statistics of the signal amplitude and the other of temporal features of the peaks of the signal amplitude. We use state-of-the-art SVM classifiers with the kernel method for both models due to its efficiency for solving classification problems that include non-linear features.

1) *Higher-order statistics classifier (HSC)*: We consider the third and fourth moments of the magnitude of the signal in terms of its skewness and kurtosis, respectively. Skewness is a measure of the lack of symmetry of a distribution, and kurtosis is a measure of whether the distribution is heavy-tailed or light-tailed relative to a normal distribution [16]. Skewness and kurtosis provide a measure of the deviation of the signal distribution from normality towards burstiness. The distribution of the amplitude when a strong radar signal is present is heavy-tailed and highly skewed to the right. On the downside, skewness and kurtosis may not be able to distinguish between the intended radar signal and similar, pulsed interference signals. In order to improve detection performance amid non-uniform bursts in the interference, we partition the signal into  $P$  contiguous partitions. Each signal partition,  $x_p$ , has a number of samples,  $N_p = \frac{N}{P}$ , where  $N$  is the number of samples of the signal. We choose  $N$  and  $P$  to produce an integer number of partitions,  $N_p$ . The kurtosis,  $\kappa_p$ , and skewness,  $\varsigma_p$ , of each partition are computed as follows,

$$\kappa_p = \frac{\frac{1}{N_p} \sum_{i=1}^{N_p} (|x_p[i]| - \overline{|x_p|})^4}{\sigma_p^4},$$

$$\varsigma_p = \frac{\frac{1}{N_p} \sum_{i=1}^{N_p} (|x_p[i]| - \overline{|x_p|})^3}{\sigma_p^3},$$

where  $\overline{(\cdot)}$  denotes the mean, and  $\sigma_p$  is the standard deviation of  $|x_p|$ . The features for this model are computed as the mean of the kurtosis and skewness over all signal partitions. Specifically,

$$\Phi_{\kappa\varsigma} = \left\{ \frac{1}{P} \sum_{p=1}^P \kappa_p, \frac{1}{P} \sum_{p=1}^P \varsigma_p \right\}.$$

2) *Peak analysis classifier (PAC)*: The peak analysis method relies on finding the peaks of the time domain signal with certain constraints. A threshold  $\gamma$  is first applied to the signal. The threshold rule ensures only peaks of a sufficient amplitude are considered for the peak search. Then, we use the second derivative test to find all the local maxima in the signal. The local maxima are further filtered by minimum separation time. This step ensures that only one sufficient peak is selected per time interval of  $T_m$ . In the last step, we limit the number of peaks by selecting the largest  $L$  peaks. We use the resulting set of peak amplitudes,  $\{\alpha_\ell\}$ , and their corresponding times,  $\{\tau_\ell\}$ , to extract the desired features for the peak analysis classifier. The differences between the times of the peaks indicate the level of uniformity of the peak separation. Specifically, the more uniform the time separation is, the higher likelihood that an in-band SPN-43 radar signal is present. Hence, we define

$\{\Delta\tau_\ell := \tau_{\ell+1} - \tau_\ell, \ell = 1, 2, 3, \dots, L-1\}$  as the set of time differences between the peaks. In addition to the statistics of the set  $\{\Delta\tau_\ell\}$ , we use the average of the peak amplitudes as one of the features. The set of features for peak analysis is defined as

$$\Phi_{\alpha\tau} = \{(\overline{\{\Delta\tau_\ell\}}), \text{var}(\{\Delta\tau_\ell\}), \max(\{\Delta\tau_\ell\}), \overline{\{\alpha_\ell\}}\},$$

where  $\text{var}(\cdot)$  is the variance, and  $\max(\cdot)$  is the maximum.

## B. Classification model

The SVM classifier constructs an optimal separating hyperplane between two linearly separable classes. Since the classes in our model are not linearly separable, we use the kernel method which expands the features into higher dimensional feature space. Specifically, we use the Gaussian kernel function. Furthermore, we tune the model hyperparameters using Bayesian optimization [17], [18]<sup>2</sup>. In particular, the hyperparameters are box-constraint and kernel-scale. The box-constraint is the regularization parameter for the soft margin of the SVM. As a result, it provides a tradeoff between misclassification and over-fitting. On the other hand, the kernel-scale regulates the influence of individual support vectors on the decision boundary. Furthermore, Platt scaling with a sigmoid function is used to map the SVM scores into class posterior probabilities [18], [19]. The probability output enables us to compute detection performance against a range of threshold values.

## IV. PERFORMANCE ANALYSIS

Field-measured signals of shipborne radar mixed with three types of interference are used to train and test the classifier. The radar and interference signals are generated separately, processed similarly to [6], and later added together in simulation. All the radar and interference signals consist of 20 ms segments, each with  $F_s = 2$  MHz. The radar signals contain 20 pulses. The interference is either WGN, a single time-division duplex (TDD) LTE signal, or ABI. Radar peak power and interference peak and average power are computed in a 1 MHz bandwidth. In addition, the signal-to-noise ratio (SNR) is defined as the peak power of the radar signal to the average noise power in 1 MHz. Field-measured radar and ABI signals are divided into two separate groups, one for training and another for evaluating detection performance. The WGN and LTE signals are generated randomly during training and testing. The TDD LTE signal configurations are selected randomly from columns of Table 1 in [6].

### A. SVM classifier training

We generated 35 200 training waveforms. Half of the set contains a radar signal plus interference and the other half contains interference only. The training set includes

<sup>2</sup>Certain commercial equipment, instruments, or materials are identified in this paper to foster understanding. Such identification does not imply recommendation or endorsement by the National Institute of Standards and Technology, nor does it imply that the materials or equipment identified are necessarily the best available for the purpose.

12800 waveforms with WGN, another 12800 waveforms with LTE interference, and 9600 waveforms with ABI. The signal state is stored in the response variable as 0 when the incumbent radar signal is absent, and as 1 when the incumbent radar signal is present. We set different levels of interference power for each scenario. For WGN, the SNR was set at (11, 13, 15, 17) dB. For LTE, the peak radar signal power was fixed at  $-89$  dBm/MHz, the required detection threshold, while the LTE power was set at  $(-100, -103, -106, -109)$  dBm/MHz.<sup>3</sup> The training waveforms with ABI were equally selected from three groups based on their peak interference to noise ratio (INR). In particular, the groups are selected based on three ranges of INR,  $(10 < \text{INR} < 20, 20 < \text{INR} < 30, \text{INR} > 30)$  dB. The SNR for the waveforms with ABI was fixed at 19 dB, which corresponds to the SNR when the peak radar signal power is at the required detection threshold and the detector has a thermal noise figure of 6 dB.

The training data was used to extract  $\Phi_{\kappa\zeta}$  features for HSC, and  $\Phi_{\alpha\tau}$  features for PAC. For the PAC model,  $T_m = 0.5$  ms,  $L = 20$ , and  $\gamma$  was set to 3 dB above the average power of the signal. The features and the response variable were fed to the SVM training algorithm. The SVM model was initially tested with 10-fold cross-validation with equal probability of the class. The confusion matrices for both classifiers are shown in Fig. 3. The percentages of correctly and incorrectly classified observations are shown in the diagonal and off-diagonal cells of the confusion matrix, respectively. In addition, the far right column and last row give the percentages of correct and incorrect classifications of each class. For example, Fig. 3(b) shows that the PAC model correctly predicts class 0 84.7% of the time. Finally, the lower right cell of each matrix shows overall accuracy. Clearly, the PAC model has higher accuracy and mis-detection rates than the HSC model.

While the confusion matrix of the cross-validation is useful for understanding overall performance and tuning the model hyperparameters, a better measure of detection performance is the receiver operating characteristic (ROC). The following ROC curves were generated with waveform data that was not used for training.

### B. Detection performance

We used the trained SVM models for HSC and PAC to evaluate ROC curves. Given the input, the trained model generates the probability of the class which is compared to a threshold to decide the presence or absence of the radar signal. We use a range of threshold values to evaluate detections and false alarms and average them over all simulation points to compute  $P_D$  versus  $P_{FA}$  curves.

1) *Signal detection in WGN*: Fig. 4 shows the ROC curves for HSC and PAC for the WGN scenario. Both classifiers require SNR of roughly 12 dB to achieve low  $P_{FA}$  at  $P_D = 0.99$ . While HSC performs better for the lower SNR

<sup>3</sup>Current CBRS requirements stipulate that commercial interference at a sensor not exceed  $-109$  dBm/MHz [3], but this analysis also considers higher levels of interference.

Output Class	Target Class $\hat{\alpha}$		
	0	1	Overall Accuracy
0	41.3%	4.9%	89.4% 10.6%
1	8.7%	45.1%	83.9% 16.1%
Overall Accuracy	82.7% 17.3%	90.2% 9.8%	86.4% 13.6%

(a) HSC

Output Class	Target Class $\hat{\alpha}$		
	0	1	Overall Accuracy
0	48.1%	8.7%	84.7% 15.3%
1	1.9%	41.3%	95.6% 4.4%
Overall Accuracy	96.2% 3.8%	82.6% 17.4%	89.4% 10.6%

(b) PAC

Fig. 3: Confusion matrix of classifiers' cross validation.

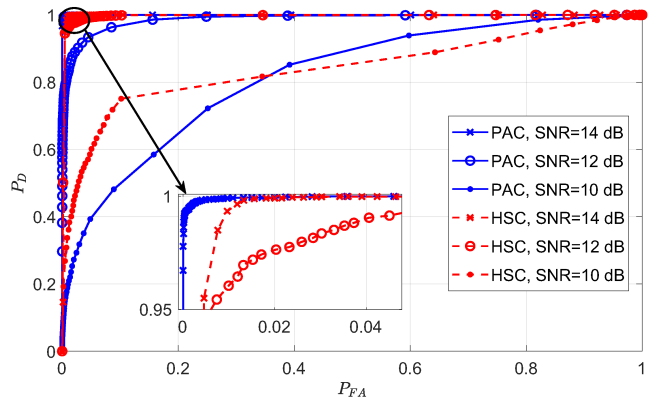


Fig. 4: Radar signal with added WGN.

values, PAC converges faster to a low  $P_{FA}$  at higher SNR. In comparison to the matched filter detector with a similar scenario [6], both HSC and PAC classifiers require about 7 dB higher SNR to achieve the same detection performance. However, considering that current detection requirements [2] equate to an SNR of about 19 dB, both HSC and PAC perform acceptably in Gaussian noise.

2) *Detection in LTE interference*: The performance of HSC and PAC in the presence of LTE interference is shown in Fig. 5. The performance of both classifiers degrades slightly from the WGN case due to relatively large variations of the LTE signal in time. Nevertheless, the performance of both detectors is still within the acceptable range since the sensors are required to tolerate  $-109$  dBm/MHz of aggregate commercial emissions [3].

3) *Detection in adjacent-band interference*: Finally, Fig. 6 shows the performance in ABI. The PAC classifier performs well for this case and not very far behind the matched filter detector for the same scenario [6]. Evidently, the HSC yields poor performance and is unreliable for this type of interference. This is not surprising since the HSC cannot distinguish between the burst of pulses of incumbent radar and ABI. This example demonstrates that a specific detector may perform well within official requirements [2] for detecting the federal incumbent radar but may perform poorly in certain realistic interference scenarios such as radar emissions from

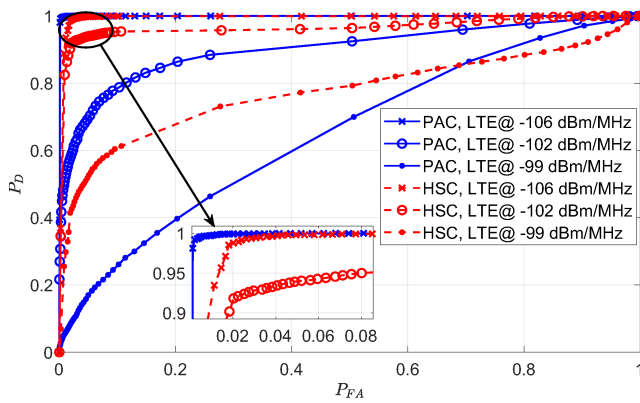


Fig. 5: Radar signal with LTE interference.

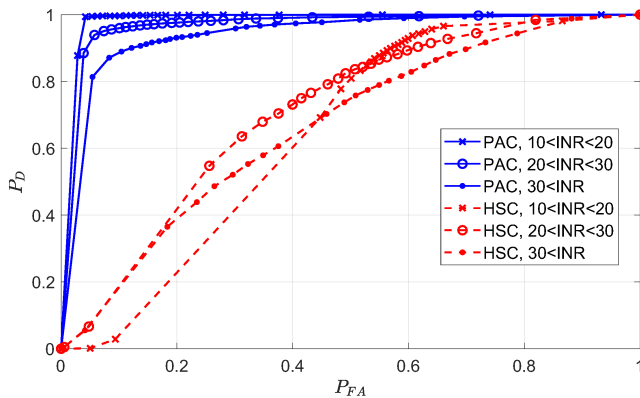


Fig. 6: Radar signal with adjacent-band radar emissions.

adjacent bands.

## V. CONCLUSION

We presented two feature-based SVM classifiers for detecting federal incumbent radar in the 3.5 GHz shared-spectrum CBRS band. We evaluated their performance using field-measured signals of the in-band incumbent radar in WGN, and in the presence of interference from dominant LTE signals or adjacent-band emissions. Although both classifiers require higher SNR values to achieve the same detection rate as the matched-filter detector, their performance is within the acceptable range of current detection requirements. In addition, the proposed SVM classifiers may provide a practical advantage since they are less computationally expensive to generalize than a matched filter for the same in-band radar signal with a partially known set of parameters. For instance, a matched-filter detector requires correlation with multiple templates if the radar pulse repetition rate is not known, while the SVM classifiers only need to be trained once with multiple templates. However, the features of the classifier should be chosen carefully since a specific detector may meet official requirements but may perform poorly in certain realistic interference scenarios such as radar emissions from adjacent bands.

## REFERENCES

- [1] "Citizens broadband radio service," 2 C.F.R. § 96, 2016.
- [2] Frank H. Sanders, John E. Carroll, Geoffrey A. Sanders, Robert L. Sole, Jeffery S. Devereux, and Edward F. Drocella, "Procedures for laboratory testing of environmental sensing capability sensor devices," Technical Memorandum TM 18-527, National Telecommunications and Information Administration, Nov. 2017.
- [3] "Requirements for commercial operation in the U.S. 3550–3700 MHz citizens broadband radio service band," Wireless Innovation Forum Document WINNF-TS-0112, Version V1.5.0, May 2018.
- [4] Paul D. Hale, Jeffrey A. Jargon, Peter J. Jeavons, Michael R. Souryal, Adam J. Wunderlich, and Mark Lofquist, "3.5 GHz radar waveform capture at Point Loma: Final test report," Technical Note 1954, National Institute of Standards and Technology, May 2017.
- [5] Paul D. Hale, Jeffrey A. Jargon, Peter J. Jeavons, Michael R. Souryal, Adam J. Wunderlich, and Mark Lofquist, "3.5 GHz radar waveform capture at Fort Story: Final test report," Technical Note 1967, National Institute of Standards and Technology, Aug. 2017.
- [6] Raied Caromi, Michael Souryal, and Wen-Bin Yang, "Detection of incumbent radar in the 3.5 GHz CBRS band," in *Proc. IEEE GlobalSIP*, Nov. 2018.
- [7] M. Bkassiny, Y. Li, and S. K. Jayaweera, "A survey on machine-learning techniques in cognitive radios," *IEEE Communications Surveys Tutorials*, vol. 15, no. 3, pp. 1136–1159, 2013.
- [8] T. O'Shea and J. Hoydis, "An introduction to deep learning for the physical layer," *IEEE Transactions on Cognitive Communications and Networking*, vol. 3, no. 4, pp. 563–575, Dec 2017.
- [9] A. Schmidt, C. Rügheimer, F. Particke, T. Mahr, H. Appel, and H. Kille, "Kurtosis based approach for detection of targets in noise," in *2016 17th International Radar Symposium (IRS)*, May 2016, pp. 1–3.
- [10] Tian-Tsong Ng, Shih-Fu Chang, and Qibin Sun, "Blind detection of photomontage using higher order statistics," in *2004 IEEE International Symposium on Circuits and Systems*, May 2004, vol. 5.
- [11] C. M. Spooner, "Classification of co-channel communication signals using cyclic cumulants," in *Conference Record of The Twenty-Ninth Asilomar Conference on Signals, Systems and Computers*, Oct. 1995, vol. 1, pp. 531–536 vol.1.
- [12] M. Petrova, P. Mähönen, and A. Osuna, "Multi-class classification of analog and digital signals in cognitive radios using support vector machines," in *2010 7th International Symposium on Wireless Communication Systems*, Sep. 2010, pp. 986–990.
- [13] M. M. Ramn, T. Atwood, S. Barbin, and C. G. Christodoulou, "Signal classification with an svm-fft approach for feature extraction in cognitive radio," in *2009 SBMO/IEEE MTT-S International Microwave and Optoelectronics Conference (IMOC)*, Nov 2009, pp. 286–289.
- [14] T. J. O'Shea, T. Roy, and T. C. Clancy, "Over-the-air deep learning based radio signal classification," *IEEE Journal of Selected Topics in Signal Processing*, vol. 12, no. 1, pp. 168–179, Feb 2018.
- [15] S. Rajendran, W. Meert, D. Giustiniano, V. Lenders, and S. Pollin, "Deep learning models for wireless signal classification with distributed low-cost spectrum sensors," *IEEE Transactions on Cognitive Communications and Networking*, vol. 4, no. 3, pp. 433–445, Sep. 2018.
- [16] "NIST/SEMATECH e-Handbook of Statistical Methods," <http://www.itl.nist.gov/div898/handbook>, April 2012.
- [17] Trevor Hastie, Robert Tibshirani, and Jerome Friedman, *The Elements of Statistical Learning*, Springer New York, second edition, 2009.
- [18] *Statistics and Machine Learning Toolbox*, The MathWorks, Inc., Natick, Massachusetts, Release 2018a, [https://www.mathworks.com/help/pdf\\_doc/stats/stats.pdf](https://www.mathworks.com/help/pdf_doc/stats/stats.pdf).
- [19] John C. Platt, "Probabilities for SV machines," in *Advances in Large Margin Classifiers*, Alexander J. Smola et al., Eds., chapter 5, pp. 61–74. MIT Press, Cambridge, Massachusetts, 2000.